DOI 10.4430/bgo00374

# Nonlinear inversion of gravity data for simple geometry anomalies using the Centred-Progressive Particle Swarm Optimisation algorithm

M. Valieghbal[1], V.E. Ardestani[2] and K. Borna[3]

[1] *Institute of Geophysics, University of Tehran, Tehran, Iran*

[2] *Center of Excellence in Survey Engineering and Disaster Management, University of Tehran, Iran*

[3] *Department of Computer Science, Faculty of Mathematics and Computer Science, Kharazmi University, Tehran, Iran*

(Received: 29 December 2020; accepted: 6 September 2021; published online: 14 February 2022)

***ABSTRACT*** Depth estimation of gravity anomalies is one of the most important geophysical problems in the exploration of mineral deposits. In the present paper, we try to estimate mass anomaly depth by using an artificial intelligence method called the Centred-Progressive Particle Swarm Optimisation (CP-PSO) with sample shapes such as a sphere, horizontal cylinder and vertical cylinder, which simulate the shape of most causative bodies. Using an artificial intelligence method is common for the case in ore bodies detection and delineation. When modelling gravity data, we estimate the depth and shape factor; therefore, we suppose depth ($z$) and shape factor ($q$) as particles in this algorithm. This technique was tested for synthetic models contaminated with random noise and the results are quite acceptable and promising. The proposed method was also successfully applied to real mineral exploration data. The desired location is near one of the outcroppings of the Safo manganese mine located in north-western Iran. The results show that the estimated depth and the shape factor model were in good agreement with the results obtained through the Euler method and drilling.

**Key words:** nonlinear inversion, simple geometric bodies, depth estimation, global optimisation methods, CP-PSO algorithm.

## 1. Introduction

Inverse modelling is the optimisation process of finding a model that is best-fitted to measuring gravity data on the Earth's surface by minimising the error function. The main purpose of solving these kinds of problems is to make information on the internal structure of the sources available. Non-uniqueness of the solution is the fundamental complication in solving these problems (Barbosa and Joao, 1994). Other extra information related to the model parameters (subsurface structures) or data parameters (statistical properties such as the Gaussian distribution) can be used to solve this complication (Jackson, 1979; Montesinos *et al*., 2005). In the inverse modelling of gravity data, two different operators exist to determine the model parameters. In the first case, if the goal is to determine the density distribution, the geometry must be assumed to be constant and a linear operator must be used. In the second case, if the goal is to determine the

 

geometric parameters of the source, the density contrast must be assumed to be constant, and a nonlinear operator must be used. Approximations, such as the Taylor expansion, may be used to turn this system into a system of linear equations (Menke, 1989; Montesinos *et al*., 2005). Global optimisation methods should be used for gravity inverse problems that include several local minima (Fernández-Martínez *et al*., 2012). In addition, prior information can be used when using these methods to solve problems (Snopek, 2005).

Using random algorithms instead of deterministic algorithms can prevent trapping in the local minima. Moreover, random algorithms are less dependent on primary assumptions.

Monte Carlo sampling methods, one of the oldest global optimisation methods based on random movements, were first used by Keilis-Borok and Yanovskaja (1967) for solving inverse problems of geophysics. Since the Monte Carlo method is very time consuming, researchers have developed various search methods for global optimisation to reduce the optimisation time. Particle swarm optimisation (PSO) is a new optimisation method that has attracted increasing research interests due to its simplicity and efficiency.

Yuan *et al.* (2008) applied ant colony optimisation (ACO) to solve the nonlinear geophysical inverse problem. They also presented a performance comparison of ACO with a genetic algorithm (GA) and simulated annealing (SA). Their results showed that the ACO method has the properties of higher speed of convergence and accuracy.

The PSO method has been applied by Fernández-Álvarez *et al*. (2006), Shaw and Srivastava (2007), and Fernández-Martínez *et al*. (2010a, 2010b).

Fernández-Martínez *et al*. (2010a) also applied the Generalised PSO (GPSO), Centred-Centered PSO (CC-PSO), and Centred-Progressive PSO (CP-PSO) to the solution and appraisal of a one-dimensional direct current resistivity inverse problem.

A full family of PSO was applied to the 2D/3D gravity inversion and model appraisal of basement relief in sedimentary basins by Pallero *et al*. (2015, 2017).

This paper aims to estimate the depth and shape of gravity anomalies with simple geometry, such as a sphere, horizontal cylinder and vertical cylinder, using CP-PSO algorithm.

## 2. Nonlinear inversion method of gravity data

In general, the gravity acceleration can be obtained from the following equation (Blakely, 1995):

$$g(P) = G \iiint_R \rho(Q) \frac{(z - \acute{z})}{r^3} dv, \tag{1}$$

where $G = 6.67 \times 10^{-11} \frac{m^3}{kg\, s^2}$ is the universal gravitational constant, *R* is the volume occupied by the mass anomaly, *P* is the observation point outside of *R* and located at (*x*, *y*, *z*), *Q* is the point of integration $(\acute{x}, \acute{y}, \acute{z})$ within *R,* and *r* is a vector directed from *Q* to *P* that is written as follows:

$$r = \sqrt{(x - \acute{x})^2 + (y - \acute{y})^2 + (z - \acute{z})^2}, \tag{2}$$

$\rho(Q)$ has the usual meaning of density.

We can write Eq. 1 as follows:

$$g(x,y,z) = \int_{\acute{z}} \int_{\acute{y}} \int_{\acute{x}} \rho(\acute{x},\acute{y},\acute{z})\varphi(x-\acute{x},y-\acute{y},z-\acute{z})\, d\acute{x}\, dy\acute{d}\acute{z}, \tag{3}$$

where

$$\varphi(x,y,z) = G\ \frac{z}{(x^2+y^2+z^2)^{3/2}}, \tag{4}$$

is a function that depends on the location of the measurement point (*P*) and underground source (*Q*).

Then,

$$g(P) = \iiint_R \rho(Q)\varphi(P,Q)dv. \tag{5}$$

The forward modelling problem is indeed calculating $g(P)$ by obtaining the values for $\rho(Q)$, $\varphi(P,Q)$ and *R* volume. In the inverse problem, $g(P)$ is a definite value and the unknowns are $\rho(Q)$ and $\varphi(P,Q)$. If $\rho(Q)$ is unknown, the problem is linear and if $\varphi(P,Q)$ is unknown, the problem is nonlinear.

Eq. 5 is difficult to solve for geologic situations with complicated geometric shapes. Therefore, we must divide the hypothetical gravitational sources into *N* simpler parts and convert Eq. 5 into something like:

$$g_m = \sum_{n=1}^{N} \rho_n \varphi_{mn}, \tag{6}$$

where $g_m$ represent the vertical attraction at the *m*-th observation point, $\rho_n$ is the density of part *n*, and $\varphi_{mn}$ is the gravitational attraction at point *m* due to part *n* with unit density.

### *2.1. Forward model*

The general new formula of a two-dimensional gravity anomaly with sample shapes such as a sphere, horizontal cylinder and vertical cylinder, along the profile over the body was summed by Essa (2010):

$$J(x_i,z) = J(0)\frac{z^{2q}}{(x_i^2+z^2)^q} \tag{7}$$

where $J(0)$ is the value of the anomaly at the origin $x_i = 0$, $z$ is the depth of the anomaly ($m$), $x_i$ is the horizontal coordinate ($m$), and $q$ is a factor roughly related to the shape factor (dimensionless) whose values for the sphere, horizontal cylinder and vertical cylinder, are 1.5, 1.0, and 0.5, respectively.

We want to use observational data to estimate the depth and shape factor of the mass anomalies. Therefore, according to Eq. 6, if $J(x_i, z)$ is a definite value and $z$ and $q$ are unknown, then, the problem is nonlinear.

### *2.2. CP-PSO, a family of Particle Swam Optimisation algorithms*

The PSO algorithm was proposed by Kennedy and Eberhart (1995). At first, it was used to simulating the social flight of birds, but after primary algorithm implementation observations, it has been applied for solving other optimisation problems. In this type of optimisation, each solution will be a bird in the space that is called a particle. Each particle has a significant value that is measured by a fitness function. In this modelling, the closer the particle is to food the better. Also, each particle has a velocity that is responsible for guiding the motion of that particle. This kind of collective artificial intelligence method is based on social psychology principles, which have many applications in computer science and other sciences. In the PSO algorithm, the collection of answers is called a swarm, and each answer is considered like a bird in a group of birds and is called a particle. Each particle contains an amount of competency that is calculated using the competency function. The direction of motion of the particles is determined by their velocity.

The PSO algorithm consists of three stages: initialisation, iteration, and termination criterion. In the first stage, the population is initialised and randomly distributed in the search space. In the iteration stage, the velocities and positions of the particles are updated by Eqs. 8 and 9, respectively. The velocity equation in PSO is (Kennedy and Eberhart, 1995):

$$\boldsymbol{v}_i^{k+1} = \omega \boldsymbol{v}_i^k + \emptyset_1\left(\boldsymbol{gbest}^k - \boldsymbol{x}_i^k\right) + \emptyset_2\left(\boldsymbol{pbest}_i^k - \boldsymbol{x}_i^k\right), \tag{8}$$

with

$$\emptyset_1 = c_1.r_1, \qquad \emptyset_2 = c_2.r_2, \qquad r_1, r_2 \in U(0,1),\ \omega, c_1, c_2 \in \mathbb{R},$$

where $\boldsymbol{x}_i^k$ is the $i$-th position of the particle in the $k$-th iteration and $\boldsymbol{v}_i^k$ is its velocity in the $k$-th iteration.

The best position of particles is represented by $\boldsymbol{pbest}_i^k$ and the best position discovered from all particles $\boldsymbol{pbest}_i^k$, is known as the global best position $\boldsymbol{gbest}^k$.

$c_1$ and $c_2$ are two positive constants that indicate the relative influence of the social components and cognition, respectively. $w$ is the inertia weight that provides a balance between local exploitation and global exploration, and $r_1$ and $r_2$ are random real values in an interval [0, 1]. The velocity of the particles on each dimension is bound by the range $[-v_{max}, v_{max}]$, and the position equation is:

$$\boldsymbol{x}_i^{k+1} = \boldsymbol{x}_i^k + \boldsymbol{v}_i^{k+1}. \tag{9}$$

If the completion criterion is met, the algorithm creates the best solution. Otherwise, the iteration process continues.

Inertia, local and global accelerations are parameters for tuning PSO.

*w* is the inertia weight that regulates the trade-off between local exploitation and global exploration. It was initially constant. However, Shi and Eberhart (1998) indicated that better results are obtained if an initial large value is considered for the inertia, in order to promote global exploration of the search space then gradually decrease it to obtain local exploitation.

Kennedy (1998) proposed values of $c_1 = c_2 = 2$ but experimental results showed that $c_1 = c_2 = 0.5$ achieved better results. Carlisle and Dozier (2001) achieved better results by choosing a larger cognitive parameter, $c_1$, than a social parameter, $c_2$, provided that $c_1 + c_2 \leq 4$. Perez and Behdinan (2007) report that a particle swarm is stable only if the following conditions are satisfied:

$$0 < c_1 + c_2 < 4$$
$$\left(\frac{c_1 + c_2}{2}\right) - 1 < \omega < 1. \tag{10}$$

If the mentioned conditions are satisfied, the system is guaranteed to converge to a local optimum value.

In this paper, we applied the CP-PSO algorithm that is fully described in the Appendix.

Modelling of gravimetric data using CP-PSO can be described as follows:

1 - we determine the main parameters related to CP-PSO. In this paper, we have considered the number of particles to be 50 and the maximum number of repetitions to be 50. In this problem, two parameters of depth and shape factor were considered as particles in the framework of the CP-PSO method;

2 - the initial population of particles in the range of motion of the input parameters is randomly generated in the search space;

3 - each particle calculates the value of the objective function corresponding to its position in space according to:

$$\frac{\|g^{obs} - g^{pre}\|}{\|g^{obs}\|} \leq tol(\%) \tag{11}$$

where $g^{obs}$ is observational data and $g^{pre}$ is predicted data by using CP-PSO algorithm;

4 - each particle identifies $\boldsymbol{pbest}$ and $\boldsymbol{gbest}$ according to its current position and the position of other particles;

5 - each particle selects a direction to move using a combination of the information in accordance with Eqs. 8 and 9;

6 - after performing the massive movement, one step of the algorithm is finished;

7 - steps 3 to 5 continue until the last iteration of the optimisation algorithm is reached;

8 - as the optimisation process converges, the optimal point is found.

All modelling and optimisation steps have been prepared by the authors in MATLAB software.

## 3. Synthetic examples

The proposed method was then used to study numerical examples. Sample shapes such as a sphere, horizontal cylinder and vertical cylinder, were selected to demonstrate the effectiveness of this technique. Synthetic models are contaminated by 3, 5, and 7% random noise. The CP-PSO swarm composed of 50 particles explored the search space with 50 iterations. The proposed method was then used to calculate the depth and shape factor.

### *3.1. Synthetic model: sphere*

The synthetic model is a sphere with a density contrast of 500 kg/m$^3$, a depth from its centre to the Earth's surface of 6 km, and a radius of 3.5 km. Using this model, we have generated synthetic gravity data contaminated by 3% random noise. The CP-PSO has to solve a two-dimensional inverse problem: shape factor and depth of anomaly. Fig. 1 shows the gravity effect of the sphere at a depth of 6 km. In this case, we repeated the algorithm 200 times to reach an answer.

It is important to highlight that CP-PSO does not use an initial model but rather adopts models based on the prior information given in the search space. The initial swarm is generated randomly in the search space. CP-PSO is able to obtain a set with all models (called equivalent models) that predict the observed data with a relative misfit lower than a given tolerance.

Fig. 2 shows histograms of each parameter's model [$q$, $z$], where $q$ is a factor related roughly to the shape of the structure (dimensionless) and $z$ is the depth of the anomaly (km).

In this case, we have used a swarm size of 50 particles and the algorithm ran 200 times.

These histograms were calculated according to the parameters of the equivalent models with an error misfit of less than 3%. The frequency distributions of the different parameters for the sphere show a wide range of solutions for $q$ and $z$.

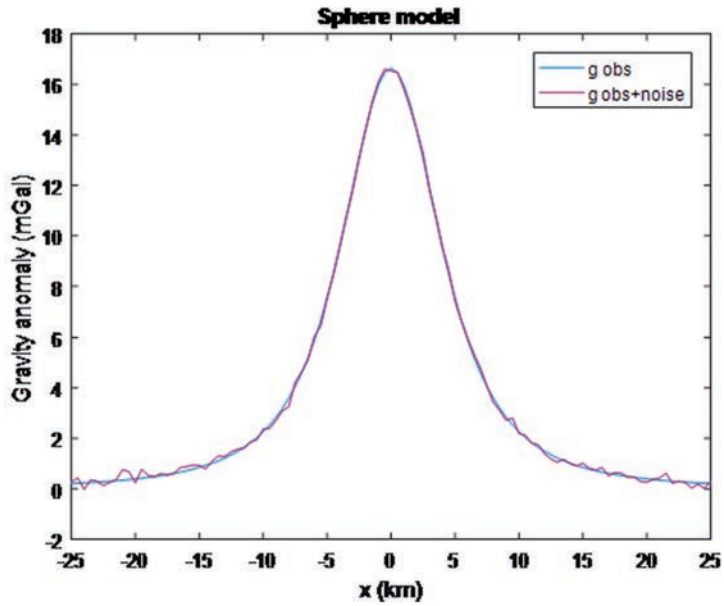


Fig. 1 - Gravity effect of a sphere at a depth of 6 km and a radius of 3.5 km.

For the histogram related to the inverted model, the frequency distribution of the shape factor is $q$ = 1.47. Therefore, our method has estimated the shape of the sphere with great accuracy. The estimated depth is $z$ = 5.9 km. To achieve these results, we employed the lower limits for the CP-PSO algorithm of $[q_{min}, z_{min}]$ = [0.5, 0.1] and $[q_{max}, z_{max}]$ = [1.5, 30] for the upper limits.

Actual and CP-PSO-estimated parameters for a spherical model are compared in Table 1.

Table 1 - Comparison of actual and CP-PSO-estimated parameters for a spherical model.

| Model parameters | Actual value | Lower bound | Upper bound | Estimated parameters |
|---|---|---|---|---|
| Shape factor ($q$) | 1.5 | 0.5 | 1.5 | 1.47 |
| Depth ($z$) in km | 6 | 0.1 | 30 | 5.9 |

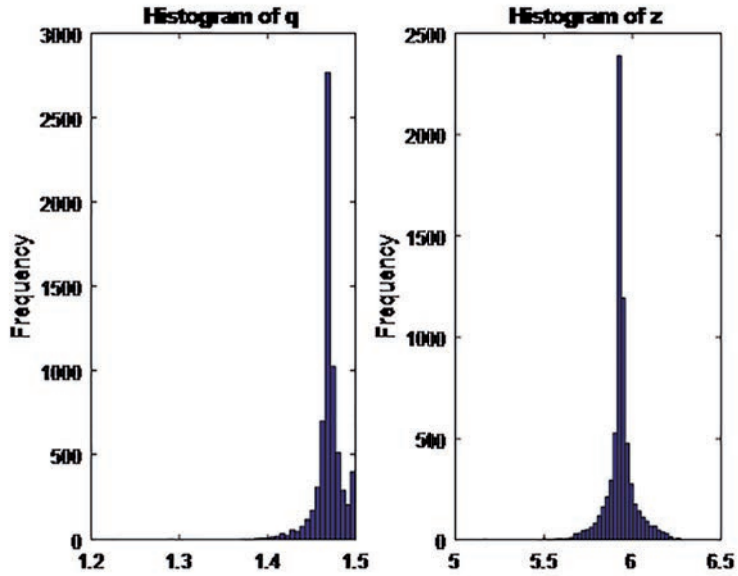


Fig. 2 - Histograms of each parameter of the model for the equivalent models with an error misfit less than 3%.

### *3.2. Synthetic model: horizontal cylinder (2D)*

The synthetic model is a horizontal cylinder with a density contrast of 650 kg/m$^3$, a depth from its centre to the Earth's surface of 43 and a radius of 8 m. Using this model, we have generated synthetic gravity data contaminated by 5% random noise. Fig. 3 shows the gravity effect of a horizontal cylinder at a depth of 43 m. Fig. 4 shows histograms of each parameter's model [$q$, $z$]. These histograms were calculated according to the parameters of the equivalent models with an error misfit of less than 4%. The frequency distribution of each model parameter (shape factor and depth) converges toward the actual value. For the histogram related to the inverted model, the frequency is $q$ = 0.94. Therefore, our method has estimated the shape of the horizontal cylinder with good accuracy. The estimated depth is $z$ = 40.3 m. To achieve these results, we employed the lower limits for the CP-PSO algorithm of $[q_{min}, z_{min}]$ = [0.5, 10] and $[q_{max}, z_{max}]$ = [1.5, 100] for the upper limits.

Actual and CP-PSO-estimated parameters for a horizontal cylinder model are compared in Table 2.

Table 2 - Comparison of actual and CP-PSO-estimated parameters for a horizontal cylinder model.

| Model parameters | Actual value | Lower bound | Upper bound | Estimated parameters |
|---|---|---|---|---|
| Shape factor (*q*) | 1 | 0.5 | 1.5 | 0.94 |
| Depth (*z*) in m | 43 | 10 | 100 | 40.3 |

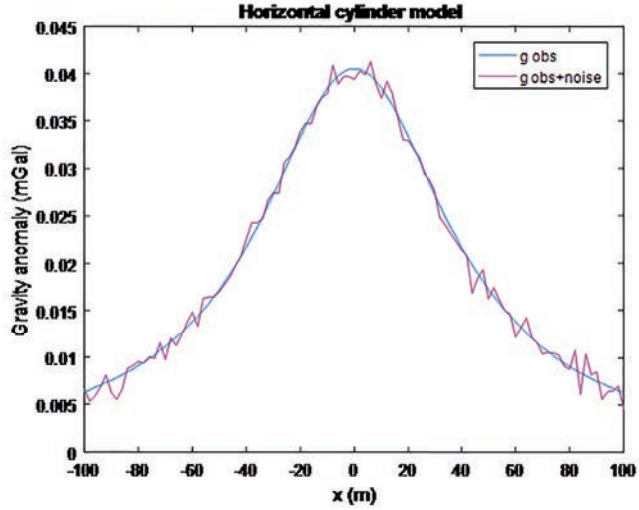


Fig. 3 - Gravity effect of a horizontal cylinder at a depth of 43 m and a radius of 8 m.

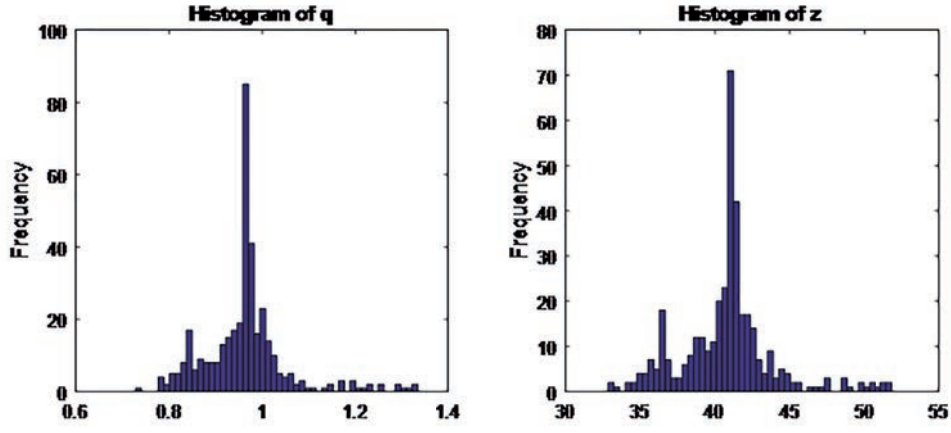


Fig. 4 - Histograms of each parameter of the model for the equivalent models with an error misfit less than 4%.

## *3.3. Synthetic model: vertical cylinder (2D)*

The synthetic model is a vertical cylinder with a density contrast of 350 kg/m$^3$, a depth from its centre to the Earth's surface of 75 and a radius of 15 m. Using this model, we have generated synthetic gravity data contaminated by 7% random noise. Fig. 5 shows the gravity effect of a

vertical cylinder at a depth of 75 m. Fig. 6 shows histograms of each parameter's model [$q$, $z$]. These histograms were calculated according to the parameters of the equivalent models with an error misfit of less than 6%. For the histogram related to the inverted model, the frequency is $q$ = 0.5. Therefore, our method has estimated the shape of the vertical cylinder with great accuracy. The estimated depth is $z$ = 67.71 m. To achieve these results, we employed the lower limits for the CP-PSO algorithm of [$q_{min}$, $z_{min}$] = [0.5, 30] and [$q_{max}$, $z_{max}$] = [1.5, 150] for the upper limits.

Actual and CP-PSO-estimated parameters for a vertical cylinder model are compared in Table 3.

Table 3 - Comparison of actual and CP-PSO-estimated parameters for a vertical cylinder model

| Model parameters | Actual value | Lower bound | Upper bound | Estimated parameters |
|---|---|---|---|---|
| Shape factor ($q$) | 0.5 | 0.5 | 1.5 | 0.5 |
| Depth ($z$) in m | 75 | 30 | 150 | 67.71 |

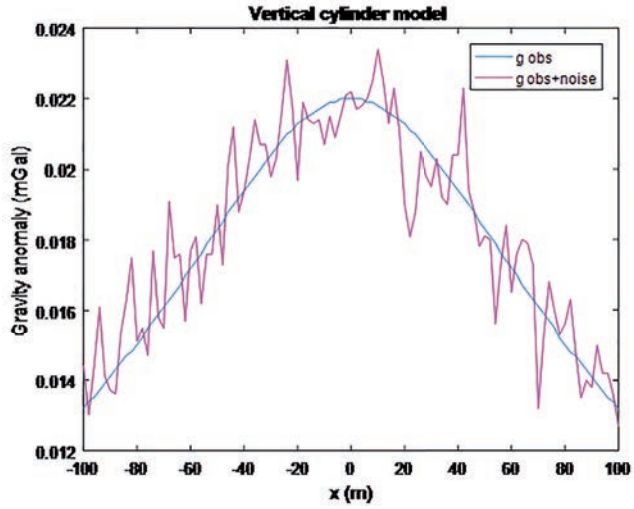


Fig. 5 - Gravity effect of a vertical cylinder at a depth of 75 m and a radius of 15 m.

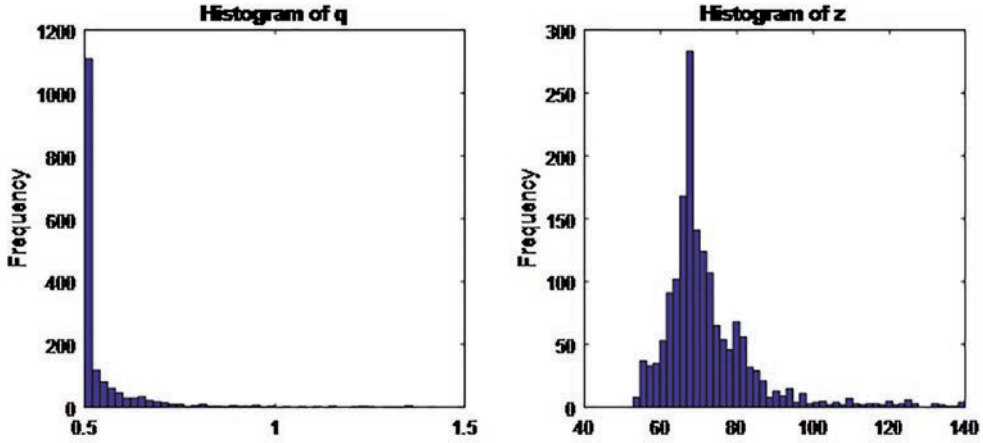


Fig. 6 - Histograms of each parameter of the model for the equivalent models with an error misfit less than 6%.

## 4. Field example

Finally, we applied this algorithm to a real dataset from the Safo manganese mine. The mine is located in the NW of Iran, 25 km north of Chaldoran. The natural position of the area relative to the city of Maku is shown in Fig. 7.

An extensive geological report of the mentioned area was made available by the Espeer company. According to the information available in the report, the dominant texture of the region is Khoy-Mako ophiolites. In this area, the Lower Cretaceous sediments are composed mostly of Orbitolina limestone and are located with transformation upon Jurassic sediments. The main outcrop on the site is made up of pelagic limestones with crags of gray to black manganese deposits. The desired location is around one of the outcrops of the Safo manganese mine and is located in a rectangle whose SW corner has the coordinates 438276 and 4342971 and whose NE corner has the coordinates 438609 and 4343187 (image system UTM). However, less gravimetric data has been harvested from the north-eastern corner of the network due to the topographic configuration in this area.

Data were acquired using a Scintrex CG3 gravimeter with an accuracy of 5 µGal including about 604 stations at 5 to 10 m intervals along with profiles with a distance between them of 2.7 m.

In order to correct the drift in the gravity measures, the amount of g is measured in a base station every two hours. A profile perpendicular to the anomaly mass was selected to estimate the depth of the mineral in this range and the depth was estimated by the method presented in this paper.

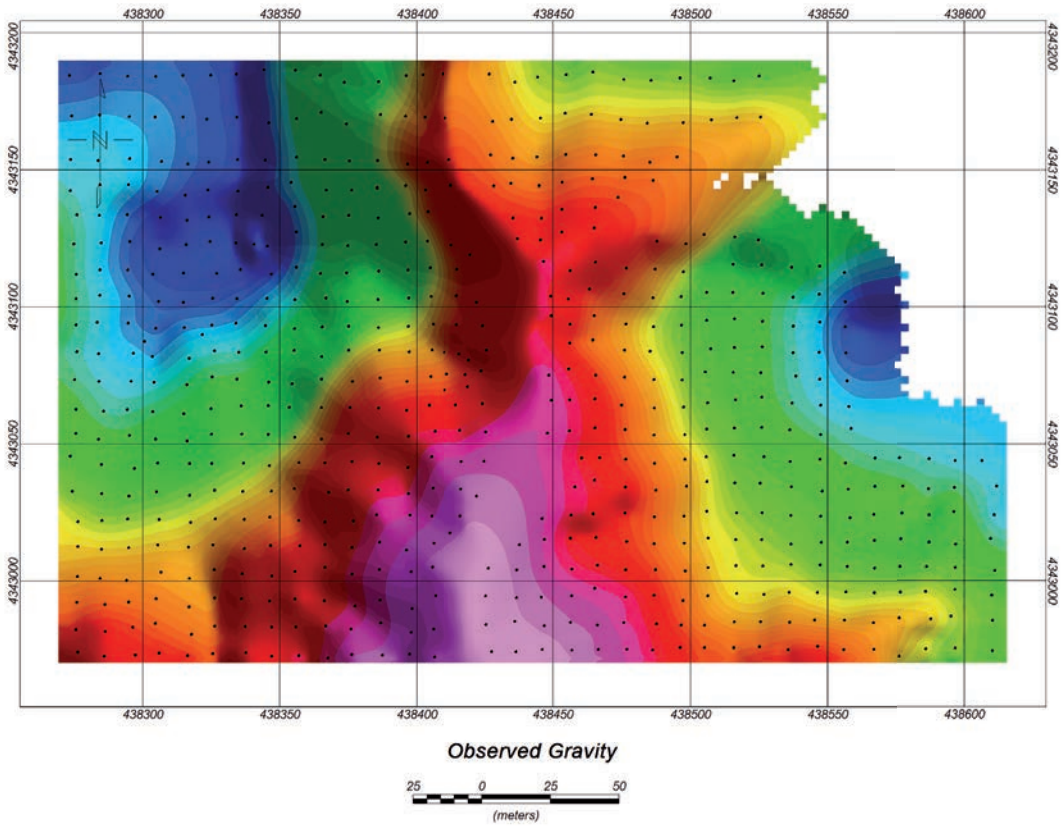


Fig. 7 - The natural position of the area relative to the city of Maku (source: Google Earth).

Fig. 8 is observed gravity and Fig. 9 shows the Digital Terrain Model (DTM). Terrain correction has been carried out through Geosoft Oasis Montaj7 using a 5 to 5 m digital terrain model and is shown in Fig. 10. Fig. 11 is the residual Bouguer anomaly map of the Safo manganese mine and the profile length is marked by a black line on the figure. The value of the used density is 2.4 g/cm$^3$. To estimate the minimum depth of this anomaly, the Euler deconvolution method is used and the results are shown in Fig. 12.

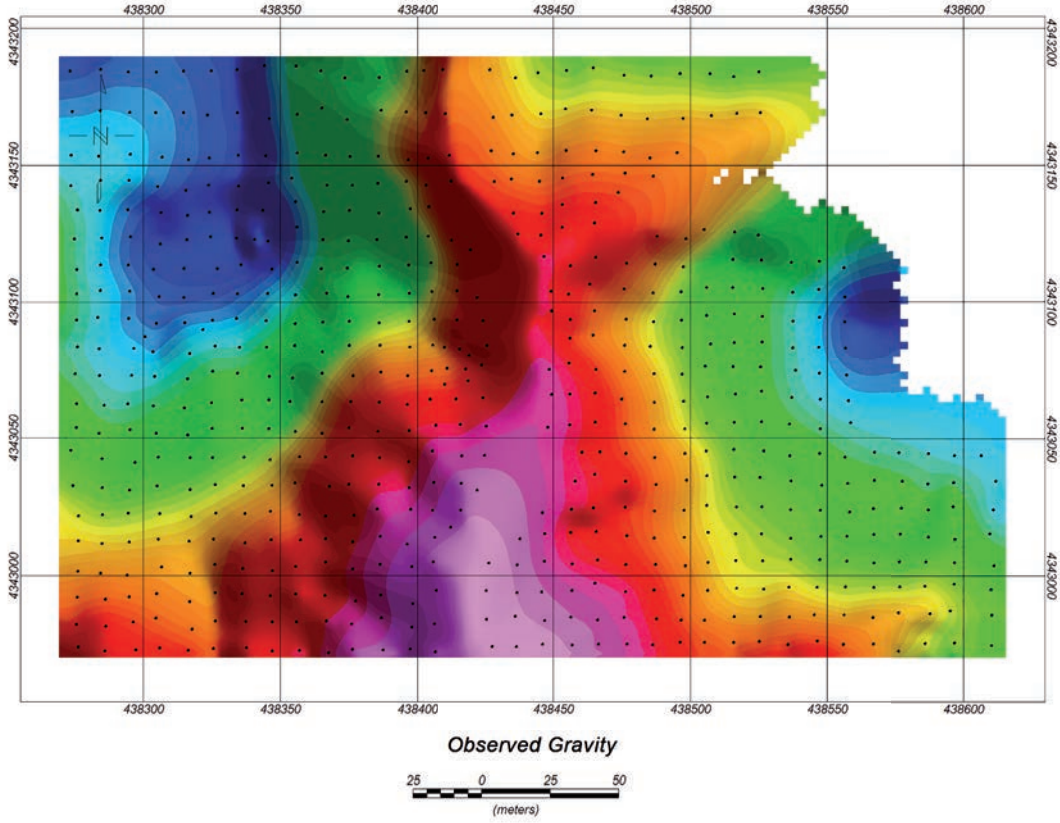


Fig. 8 - Observed gravity.

The Euler depths are computed by the following equation (Thompson, 1982):

$$(x - x_0)\frac{\partial g}{\partial x} + (y - y_0)\frac{\partial g}{\partial y} + (z - z_0)\frac{\partial g}{\partial z} = Ng \qquad (12)$$

where $x_0$, $y_0$ and $z_0$ are the coordinates of a point of the underground source and $N$ is the structural index.

As can be understood from Fig. 12, the minimum depth of the Safo manganese mine is from 5 to 25 m. Therefore, we set the range of $z$ between 1 and 100 m. According to the dimensions of particles, which include the geometrical parameter and the depth of gravity anomaly, the lower range is in the range [$q_{min}$, $z_{min}$] = [0.5, 1] and we consider the upper limit

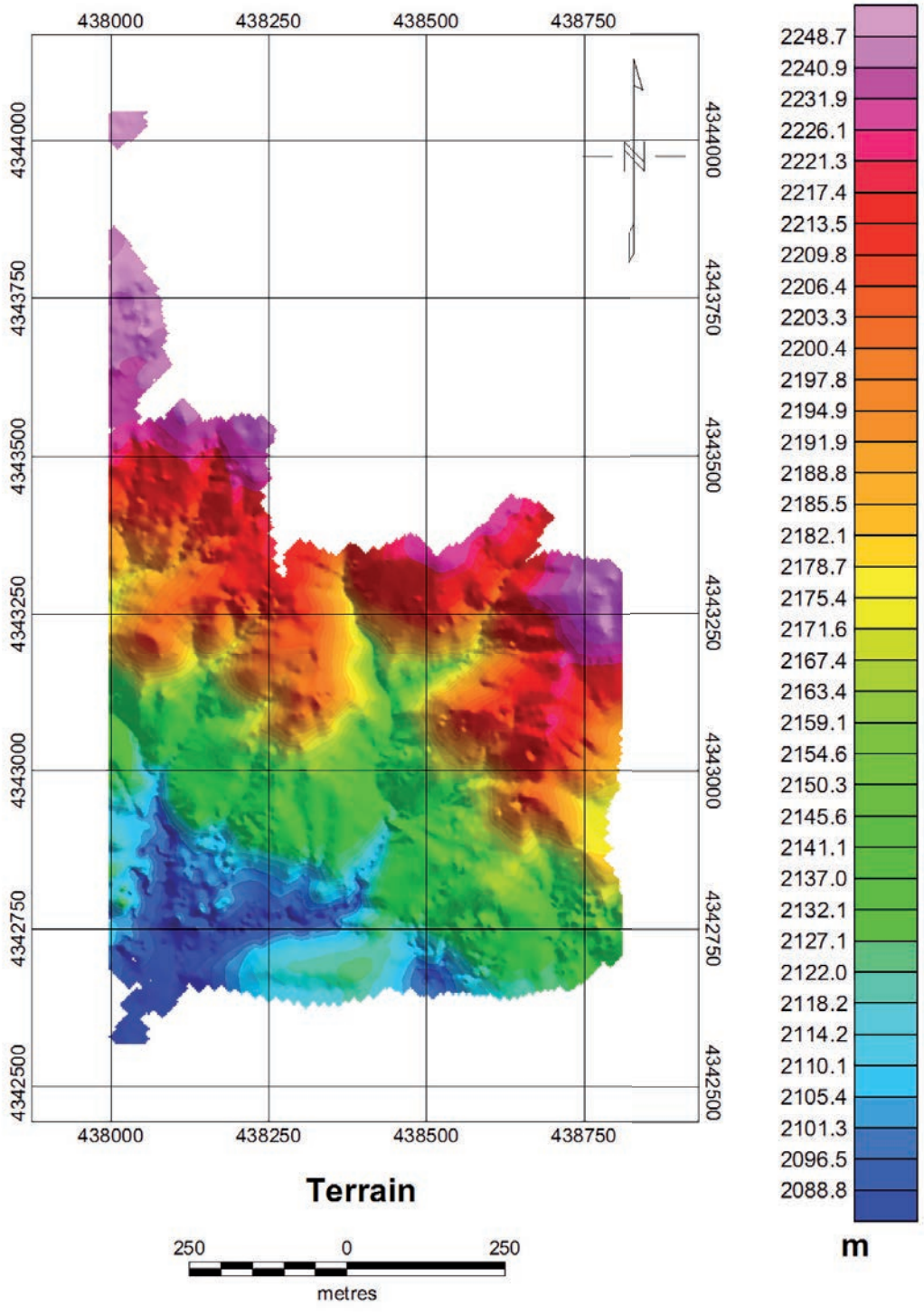


Fig. 9 - Digital Terrain Model (DTM).

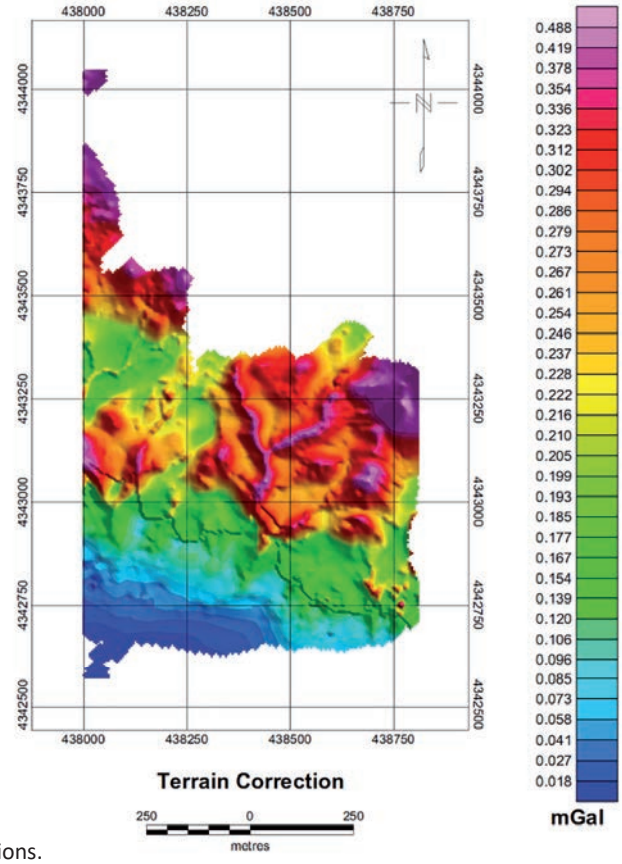


Fig. 10 - Terrain corrections.

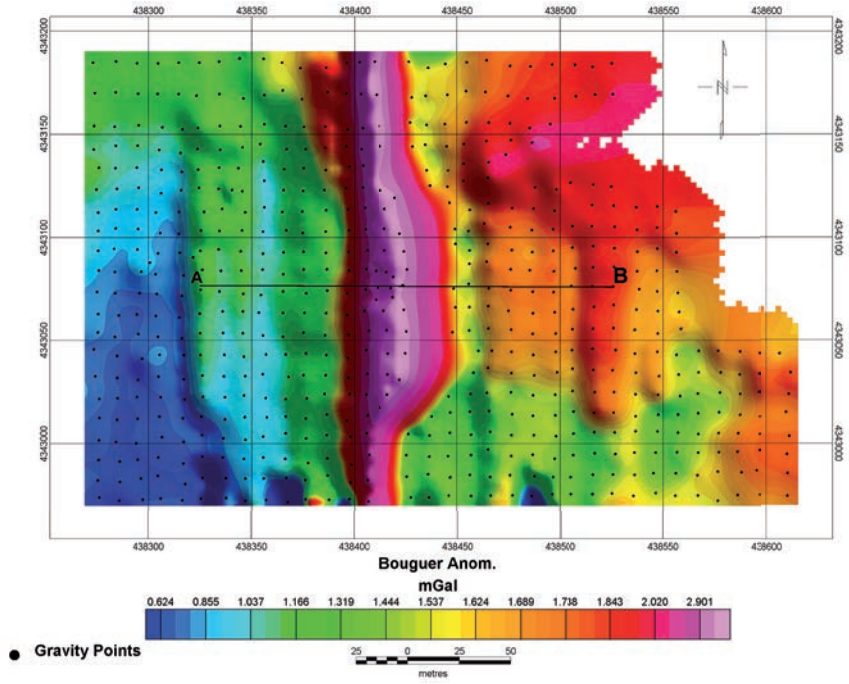


Fig. 11 - The residual Bouguer anomaly map of the Safo manganese mine.

[$q_{max}$, $z_{max}$] = [1.5, 100]. Fig. 13 shows the observed and predicted residual gravity anomaly of the Safo manganese mine. Fig. 14 shows histograms of each parameter model [$q$, $z$]. These histograms are calculated according to the parameters of the equivalent models with an error misfit of less than 4%. For the histogram related to the inverted model, the frequency is $q$ = 0.81 and $z$ = 24.03 m.

As can be seen in Fig. 11, there is an obvious mineral elongation in the N-S direction. Simple models such as a sphere, horizontal cylinder and vertical cylinder, may not be geologically realistic but are usually sufficient to analyse many sources of isolated anomalies (Abdelrahman and El-Araby, 1993).

The Euler deconvolution method is used to estimate the minimum depth of this anomaly and the results are shown in Fig. 12. From this figure, it is observed that the western wall of the anomaly is located at a minimum depth of approximately 5 to 10 m and the eastern wall of the anomaly is located at a minimum depth of approximately 10 to 20 m.

The estimated shape and depth of the surface anomaly are also in good agreement with the drilling results. One of the advantages of global optimisation methods is to obtain the uncertainty of the obtained models. With attention to random processes in model upgrades, a new model that is somewhat different from the previous model, is obtained with each run of the program. In this paper, the uncertainty in real data was obtained by running the CP-PSO algorithm 50 times

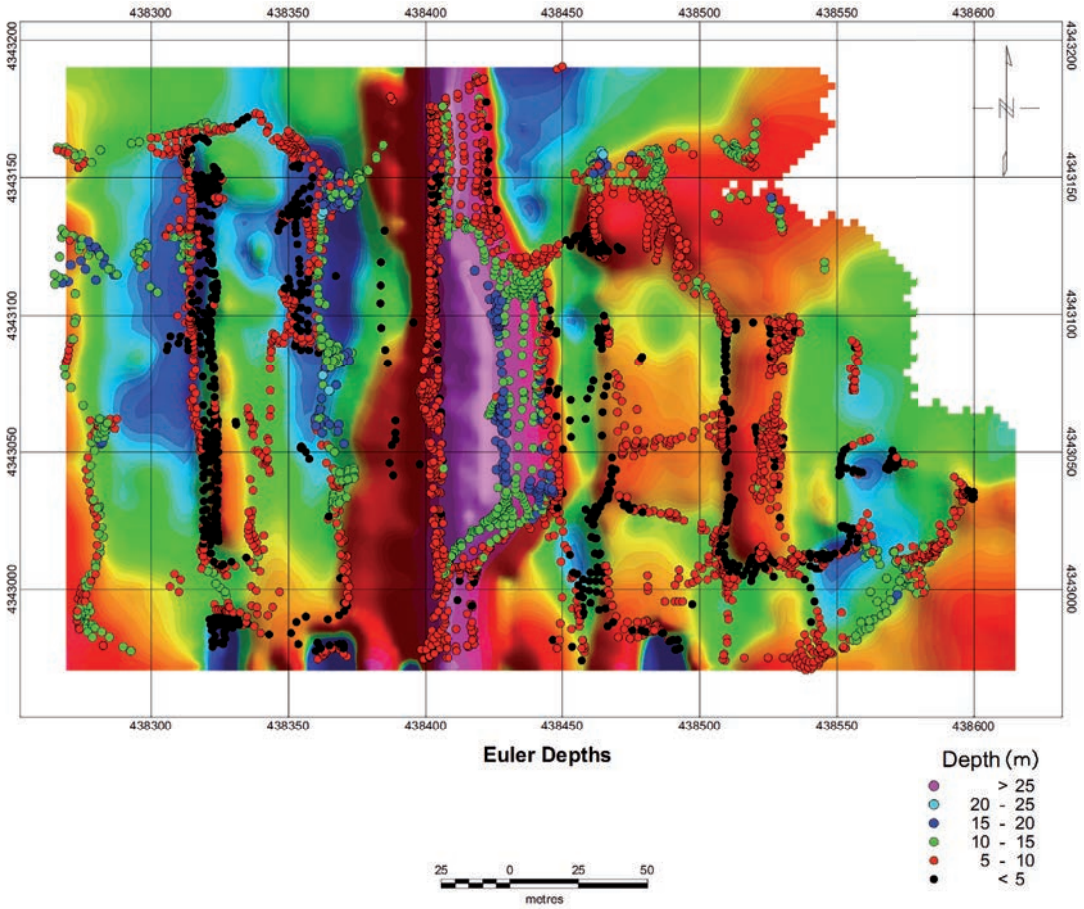


Fig. 12 - Estimated depth by Euler deconvolution method (m).

and results were obtained in 50 different models. Fig. 15 shows the percentage of relative misfit and the swarm dispersion with the number of iterations. As can be seen in the figure, the misfit rapidly decreases with the iterations and its exploratory behaviour can be observed in iterations 47 and 50 where the misfit increases and is higher than 20%. Global Search (Exploration) means the ability of the algorithm to explore different areas of the search spaces. The dispersion swarm in Fig. 15 shows that it is never lower than 4%. Fig. 16 shows the percentage in equivalent models with the considered percentage of error misfit. We found that more than 56% of the inverted models or 1407 models had an error misfit of less than 5% and that percentage increased to around 76% of the inverted models or 1924 models if the error misfit was increased to 10%.

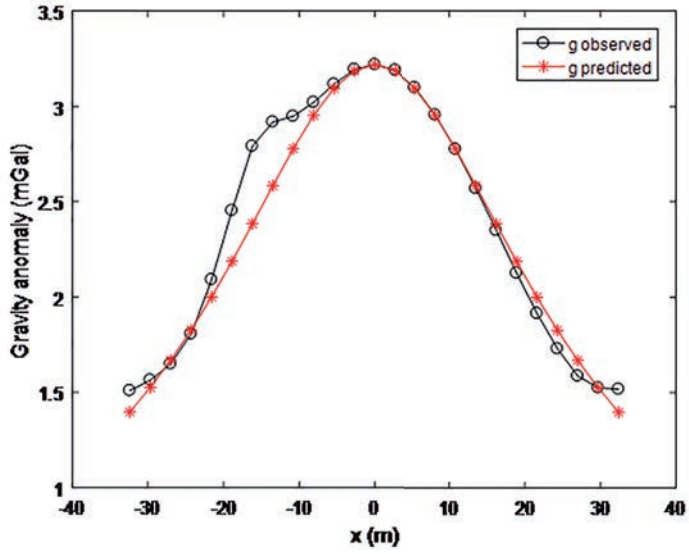


Fig. 13 - The observed and predicted residual gravity anomaly at the Safo manganese mine.

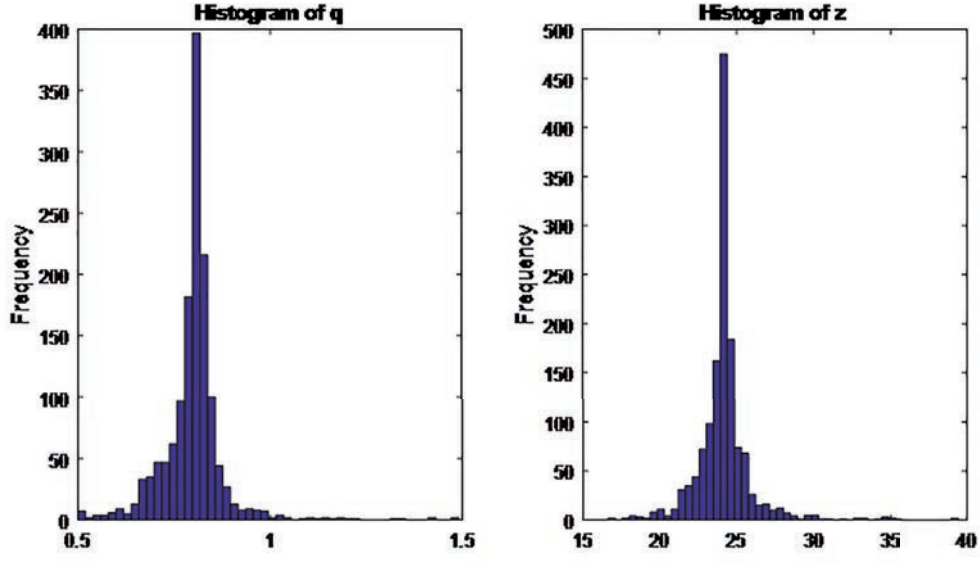


Fig. 14 - Histograms of each parameter of the model for the equivalent models with an error misfit less than 4%.

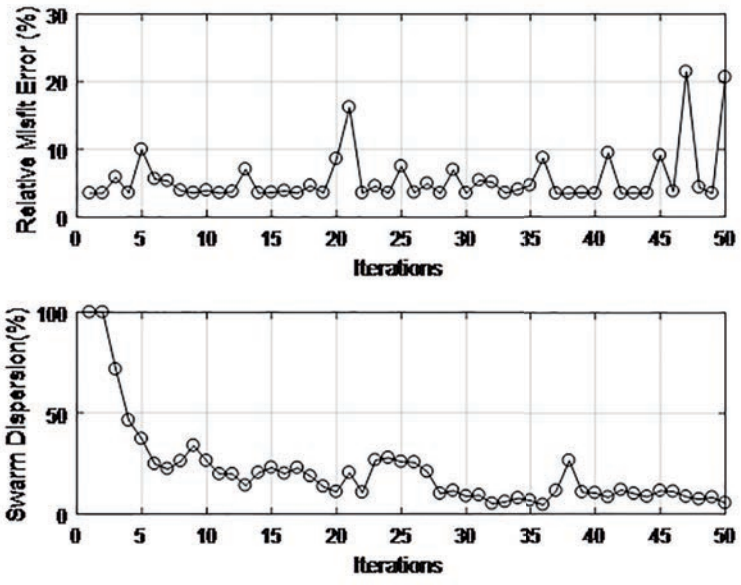


Fig. 15 - Percentage of relative misfit and the swarm's ability to explore in each iteration.

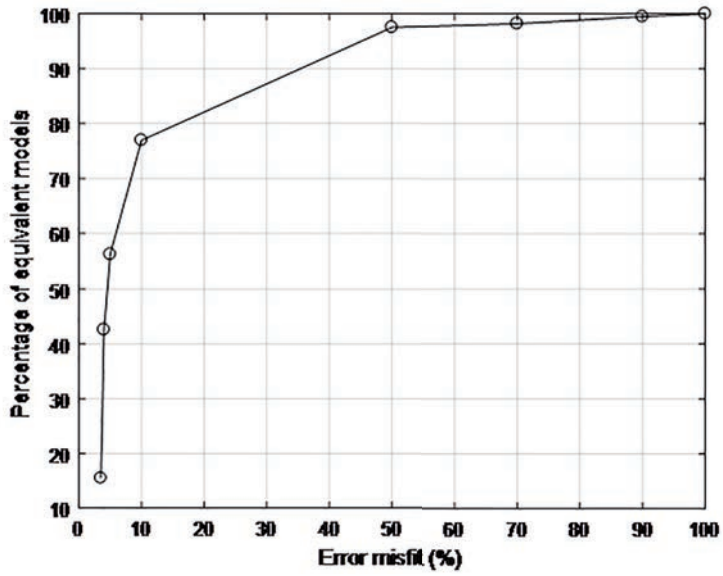


Fig. 16 - Percentage of equivalent models with the considered percentage of error misfit.

## 5. Drilling results

Fig. 17 shows the location of the exploration range on the 1:250,000 geological map. Ten trenches and ten wells with a total area of 357 $m^2$ and 21 $m^2$ were drilled in this mine.

Fig. 18 shows the legend for the Safo manganese exploration range that was prepared based on field surveys and thin section studies.

The exploration program has led to the identification of five indices containing minerals (a total of 14 mineral patches) in different areas of the range. The specifications of these indices, labelled with codes A, B, C, D, and E are shown in Table 4.

Table 4 - The specifications of mineralised areas detected during the preliminary exploration phase.

| Mineral Indices | Height level (m) | Geographical coordinates | | Mineral patches | Outcrop dimensions ($m^2$) | Area ($m^2$) | Mineral Reserve (ton) |
|---|---|---|---|---|---|---|---|
| | | Longitude (DMS) | Latitude (DMS) | | | | |
| A | 2200 | 44° 16 ‘ 15″ | 39° 14′ 22.8″ | A1 | 35×18 | 630 | 2213 |
| | | | | A2 | 65×15 | 975 | 2643 |
| B | 2220 | 44° 17′ 12″ | 39° 14′ 06″ | B1 | 25×25 | 625 | 45162 |
| | | | | B2 | 15×15 | 225 | 224 |
| | | | | B3 | 15×15 | 225 | - |
| | | | | B4 | 17×6 | 102 | - |
| C | 2220 | 44° 17′ 19.2″ | 39° 14′ 02.5″ | C1 | 20×20 | 400 | 803 |
| | | | | C2 | 15×7 | 105 | 1621 |
| | | | | C3 | 17×6 | 102 | 977 |
| | | | | C4 | 12×4 | 48 | - |
| D | 2210 | 44° 16′ 46.2″ | 39° 14′ 14.4″ | D1 | 70×2 | 140 | 184 |
| E | 2220 | 44° 17′ 47.4″ | 39° 14′ 14.4″ | E1 | 80×2.5 | 200 | 2781 |
| | | | | E2 | 40×1.5 | 60 | |
| | | | | E3 | 50×2.5 | 125 | |

Finally, after performing the final calculations to determine the mineral reserves in this section, 56,608 tons of mineral with an average grade of 30.06% manganese (equivalent to the total content of 17,016 tons of manganese oxide) was estimated.

The minimum depth needed to calculate the amount of reserve for most patches is 5 m and at greater depths, the amount of reserves can reach up to 80,000 tons.

The mineral outcrop related to patch A1 is shown in Fig. 19.

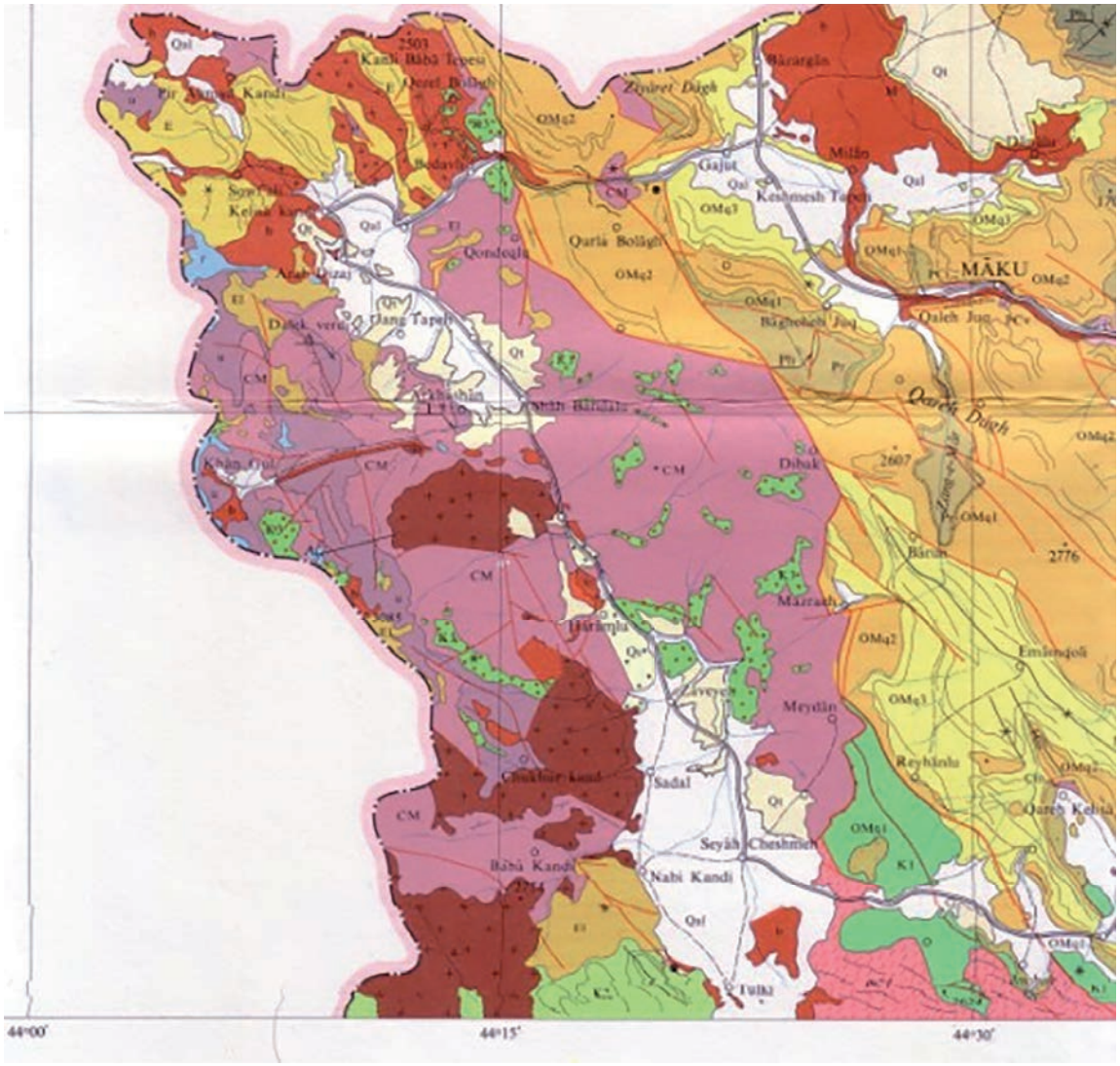


Fig. 17 - The location of the exploration range on a 1:250,000 geological map.

## 6. Conclusions

In the present study, the CP-PSO algorithm was used to interpret the gravity data for a simple buried structure, such as a vertical cylinder, a horizontal cylinder or a sphere. Using random algorithms instead of deterministic algorithms can prevent trapping in the local minimums. Random algorithms are also less dependent on primary assumptions.

In this modelling, two parameters of depth and shape factor were considered as particles in the framework of the CP-PSO method and the maximum and minimum depth was used for the prior information. Like other inversion methods that overcome the non-uniqueness problem by constraints, we used depth and shape factor constraints for this purpose. The method was then tested for synthetic models with random noise. The technique was also successfully applied

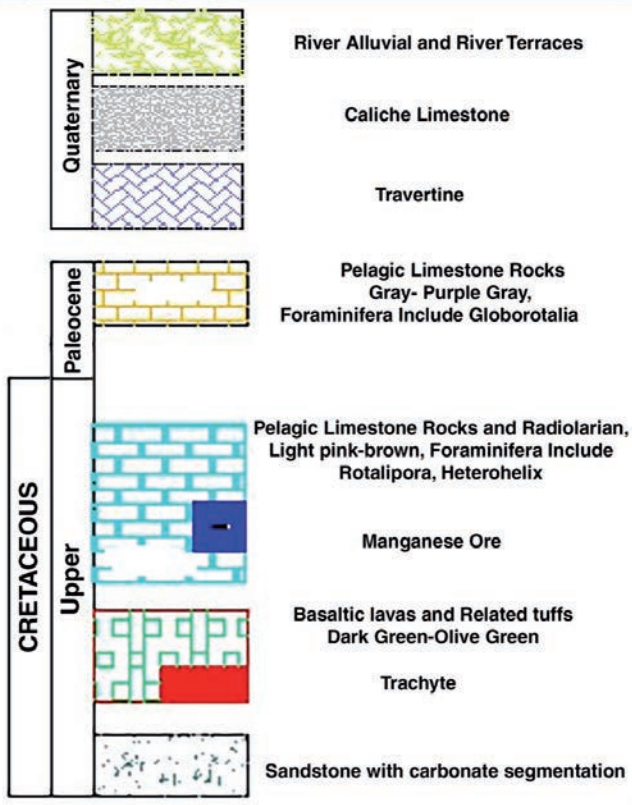


Fig. 18 - Legend prepared based on field surveys and thin section studies for the Safo manganese exploration range.

Fig. 19 - Mineral outcrop related to patch A1.

to real mineral exploration data. The desired location was one of the outcroppings of the Safo manganese mine and located in north-western Iran. An anomaly identified at a depth of 24.06 m had a good fit with the drilling results.

REFERENCES

Abdelrahman E.S.M. and El-Araby T.M.; 1993: *A least-squares minimisation approach to depth determination from moving average residual gravity anomalies*. Geophys., 58, 1779-1784.

Barbosa V.C.F. and Joao B.; 1994: *Generalized compact gravity inversion*. Geophys., 59, 57-68.

Blakely R.J.; 1995: *Potential theory in gravity and magnetic applications*. Cambridge University Press, Cambridge, United Kingdom, 461 pp., doi: 10.1017/CBO9780511549816.

Carlisle A. and Dozier G.; 2001: *An off-the-shelf PSO*. In: Proc. The Workshop on Particle Swarm optimisation, Indianapolis, IN, USA, Vol. 1, pp. 1-6.

Essa K.S.; 2010: *A generalized algorithm for gravity or self-potential data inversion with application to mineral exploration*. In: Expanded Abstracts 21st Conference and Exhibition, Australian Society of Exploration Geophysicists (ASEG), Innovations in Geophysical Inversion, Sidney, Australia, pp. 1-4.

Fernández-Álvarez J.P., Fernández-Martínez J.L., García-Gonzalo E. and Menéndez-Pérez C.O.; 2006: *Application of the particle swarm optimisation algorithm to the solution and appraisal of the vertical electrical sounding inverse problem*. In: Proc. 11th Annual Conference of the International Association of Mathematical Geology (IAMG'06), Liège, Belgium, pp. 3-8.

Fernández-Martínez J.L. and García-Gonzalo E.; 2009: *The PSO family: deduction, stochastic analysis and comparison*. Swarm Intell., 3, 245-273.

Fernández-Martínez J.L., García-Gonzalo E., Fernández-Álvarez J.P., Kuzma H.A. and Menéndez-Pérez C.O.; 2010a: *PSO: a powerful algorithm to solve geophysical inverse problems. Application to a 1D-DC resistivity case*. J. Appl. Geophys., 71, 13-25, doi: 10.1016/j.jappgeo.2010.02.001.

Fernández-Martínez J.L., García-Gonzalo E. and Naudet V.; 2010b: *Particle swarm optimisation applied to solving and appraising the streaming-potential inverse problem*. Geophys., 75, WA3-WA15.

Fernández-Martínez J.L., Mukerji T., García-Gonzalo E. and Suman A.; 2012: *Reservoir characterisation and inversion uncertainty via a family of particle swarm optimizers*. Geophys., 77, M1-M16, doi: 10.1190/geo2011-0041.1.

Jackson D.D.; 1979: *The use of priori data to resolve non-uniqueness in linear inversion*. Geophys. J. R. Astron. Soc., 57, 137-157.

Keilis-Borok V.I. and Yanovskaja T.B.; 1967: *Inverse problems of seismology (structural review)*. Geophys. J. Int., 13, 223-234.

Kennedy J.; 1998: *The behavior of particles*. In: Proc. 7th International Conference on Evolutionary Programming, San Diego, CA, USA, pp. 581-589, doi: 10.1007/BFb0040809.

Kennedy J. and Eberhart R.C.; 1995: *Particle swarm optimisation*. In: Proc. IEEE International Conference on Neural Networks, Perth, WA, Australia, Vol. 4, pp. 1942-1948, doi: 10.1109/ICNN.1995.488968.

Menke W.; 1989: *Geophysical data analysis: discrete inverse theory*. Academic Press Inc., Cambridge, MA, USA, 289 pp.

Montesinos F.G., Arnoso J. and Vieira R.; 2005: *Using a genetic algorithm for 3D inversion of gravity data in Fuerteventura (Canary Islands)*. Int. J. Earth Sci., 92, 301-316.

Pallero J.L.G., Fernández-Martínez J.L., Bonvalot S. and Fudym O.; 2015: *Gravity inversion and uncertainty assessment of basement relief via Particle Swarm Optimisation*. J. Appl. Geophys., 116, 180-191.

Pallero J.L.G., Fernández-Martínez J.L., Bonvalot S. and Fudym O.; 2017: *3D gravity inversion and uncertainty assessment of basement relief via Particle Swarm Optimisation*. J. Appl. Geophys., 139, 338-350.

Perez R.L. and Behdinan K.; 2007: *Particle swarm approach for structural design optimisation*. Comput. Struct., 85, 1579-1588.

Shaw R. and Srivastava S.; 2007: *Particle swarm optimisation: a new tool to invert geophysical data*. Geophys., 72, F75-F83.

Shi Y. and Eberhart R.C.; 1998: *Parameter selection in particle swarm optimisation*. In: Proc. 7th International Conference on Evolutionary Programming, San Diego, CA, USA, pp. 591-600.

Snopek K.; 2005: *Inversion of gravity data with application to density modeling of the Hellenic subduction zone*. Ph.D. Thesis, Department of Geosciences at the Ruhr University, Bochum, Germany, 2 pp.

Thompson D.T.; 1982: *EULDPH: a new technique for making computer-assisted depth estimates from magnetic data*. Geophys., 47, 31-37.

Yuan S., Tian N., Chen Y., Liu H. and Liu Z.; 2008: *Nonlinear geophysical inversion based on ACO with hybrid techniques*. In: Proc. 4th International Conference on Natural Computation (ICNC'08), Jinan, China, Vol. 4, pp. 530-534.

*Corresponding author:* Marzieh Valieghbal
Institute of Geophysics, University of Tehran
Northern Karegar str., Tehran, Iran
Phone: +98 992 3491141; e-mail: valieghbalm@ut.ac.ir

## Appendix: The CP-PSO algorithm

The CP-PSO algorithm is one of the explorative members of the PSO family that Fernández-Martínez and García-Gonzalo (2009) considered a PSO continuous model. Where the oscillation centre may be delayed at time $t_0$ with respect to the trajectory $\boldsymbol{x}_i(t)$:

$$\boldsymbol{x}_i''(t) + (1-\omega)\,\boldsymbol{x}_i'(t) + \emptyset \boldsymbol{x}_i(t) = \emptyset_1 \boldsymbol{gbest}(t-t_0) + \emptyset_2 \boldsymbol{pbest_i}(t-t_0), \qquad t, t_0 \in \mathbb{R} \tag{A1}$$

where:

$$\emptyset = \emptyset_1 + \emptyset_2$$

In order to discretise the model A1, a centred discretisation in acceleration and velocity are used in Eq. A2:

$$\begin{aligned} x'(t) &\simeq \frac{x(t+\Delta t) - x(t)}{\Delta t}, \\ x''(t) &\simeq \frac{x'(t) - x'(t-\Delta t)}{\Delta t}, \end{aligned} \tag{A2}$$

Replacing the finite difference schemes (Eq. A2) in the PSO continuous model (Eq. A1) Fernández-Martínez and García-Gonzalo (2009) arrive at the following relationship for the velocity:

$$\begin{aligned} v(t) = \frac{v(t-\Delta t)}{1 + (1-\omega)\Delta t} + \frac{\emptyset_1 \Delta t}{1 + (1-\omega)\Delta t}(gbest(t-t_0) - x(t)) \\ + \frac{\emptyset_2 \Delta t}{1 + (1-\omega)\Delta t}(pbest(t-t_0) - x(t)), \end{aligned} \tag{A3}$$

then:

$$v(t+\Delta t) = \frac{v(t)}{1+\ (1-\omega)\Delta t} + \frac{\emptyset_1 \Delta t}{1+\ (1-\omega)\Delta t}\big(gbest(t+\Delta t - t_0) - x(t+\Delta t)\big) + \frac{\emptyset_2 \Delta t}{1+\ (1-\omega)\Delta t}\big(pbest(t+\Delta t - t_0) - x(t+\Delta t)\big), \tag{A4}$$

Taking into account that

$$x(t+\Delta t) = x(t) + v(t)\Delta t, \tag{A5}$$

the following equations show the CP-PSO algorithm with delay $t_0$:

$$v(t+\Delta t) = \frac{1-\emptyset\Delta t^2}{1+(1-\omega)\Delta t} v(t) + \frac{\emptyset_1 \Delta t}{1+(1-\omega)\Delta t}\big(gbest(t+\Delta t - t_0) - x(t)\big) + \frac{\emptyset_2 \Delta t}{1+(1-\omega)\Delta t}\big(pbest(t+\Delta t - t_0) - x(t)\big) \tag{A6}$$

$$x(t+\Delta t) = x(t) + v(t)\Delta t, \qquad t, \Delta t \in \mathbb{R}, \qquad x(0) = x_0, \qquad v(0) = v_0 \tag{A7}$$

For the CP-PSO algorithm, $\Delta t = t_0$ therefore, the equations simplify to (Fernández-Martínez and García-Gonzalo, 2009):

$$v(t+\Delta t) = \frac{1-\emptyset\Delta t^2}{1+\ (1-\omega)\Delta t} v(t) + \frac{\emptyset_1 \Delta t}{1+\ (1-\omega)\Delta t}\big(gbest(t) - x(t)\big) + \frac{\emptyset_2 \Delta t}{1+(1-\omega)\Delta t}\big(pbest(t) - x(t)\big), \tag{A8}$$

$$x(t+\Delta t) = x(t) + v(t)\Delta t, \qquad t, \Delta t \in \mathbb{R}, \qquad x(0) = x_0, \qquad v(0) = v_0. \tag{A9}$$